THE UNIVERSITY of EDINBURGH

Edinburgh Research Explorer

A CFD investigation with high-resolution grids of downwind sail aerodynamics

Citation for published version:
Viola, IM & Ponzini, R 2011, 'A CFD investigation with high-resolution grids of downwind sail aerodynamics' Paper presented at Developments in Marine CFD, London, United Kingdom, 23/03/11 - 24/03/11, pp. 99-109.

Link:
Link to publication record in Edinburgh Research Explorer

Document Version:
Peer reviewed version

General rights
Copyright for the publications made accessible via the Edinburgh Research Explorer is retained by the author(s) and / or other copyright owners and it is a condition of accessing these publications that users recognise and abide by the legal requirements associated with these rights.

Take down policy
The University of Edinburgh has made every reasonable effort to ensure that Edinburgh Research Explorer content complies with UK legislation. If you believe that the public display of this file breaches copyright please contact openaccess@ed.ac.uk providing details, and we will remove access to the work immediately and investigate your claim.

Download date: 05. Apr. 2019

A CFD INVESTIGATION WITH HIGH-RESOLUTION GRIDS OF DOWNWIND SAIL AERODYNAMICS

IM Viola School of Marine Science and Technology, Newcastle University, UK
R Ponzini High-Performance Computing Group, CILEA Consortium, Milan, Italy

SUMMARY

The aerodynamics of an America's Cup yacht - sailing downwind - was investigated with different grids and numerical schemes. From 170,000 cells to more than one billion cells were used. The high grid resolution squeezed the role of the turbulence model and simulations both with and without it were performed. The computed forces were compared with wind tunnel data. Being the first time that a grid of more than one billion cells is achieved on a complex three-dimensional geometry, the meshing procedure and the high-performance computing environment are described in details. The one-billion-cell simulations run on 512 CPUs for about 170 hours using 2 TB of RAM.
While the simulations performed without turbulence model did not showed a consistent trend increasing the grid resolution, the simulations performed with the turbulence model showed a consistent force overestimation, as reported by other authors on similar geometries, and the numerical/experimental differences decreased increasing the grid resolution.

1. INTRODUCTION

Computational Fluid Dynamics (CFD) has been widely used to understand the aerodynamics of sailing yachts. Most of the studies are commercial investigations with the primary aim to set up an operative design tool. CFD is today commonly used to predict aerodynamic forces, which allow Velocity Prediction Programs to be run for performance optimization [1]. Numerical simulations are also used to compare sail designs and to optimize sail parameters [2, 3].
Most of CFD applications for design purposes are based on the Reynolds-Averaged Navier-Stokes (RANS) equations, which allow the complexity of turbulent flow to be dealt without resolving all of the turbulent scales, and thus avoid most of the computational costs required by a direct numerical simulation (DNS).
A yacht sailing upwind (i.e. heading for a point upwind its position) uses sails with small camber trimmed near the maximum lift/drag ratio, while a yacht sailing downwind (i.e. heading for a point downwind its position), uses deep sails, such as the spinnaker, trimmed close to the maximum lift.
Numerical computations on upwind sails have been performed since the 1960s with inviscid models [4, 5, 6], and these are still widely used. Upwind sails do not show a large amount of separated flow and the sail performance can be adequately predicted, even neglecting the viscosity effects. The main advantage of inviscid codes is the smaller computational effort required, which permits them to be efficiently coupled with structural models for simulating sail deformation [7]. Unfortunately, when upwind sails are trimmed to maximize the driving force under light wind conditions, strong flow separation occurs [8]. Under these conditions inviscid models over-predict the driving force because they can not take account of viscous separation. On the contrary, RANS models show better agreement with experimental data for upwind sail aerodynamic forces [9].
Indeed viscous models are an issue not only when upwind sails are modelled under light wind conditions, but also when any downwind condition is modelled. Downwind sail aerodynamics deals with high-lift partially separated flow.
Hedges performed the first RANS simulation on downwind sails in the early 1990s [10, 11]. The increasing computational capability of recent years has induced many authors to use RANS models to simulate the aerodynamics of downwind sails. A comprehensive review of these publications can be found in [12]. A numerical versus experimental comparison is normally conducted only in terms of global forces - usually measured with a force balance placed under the boat model. In recent publications [13, 14, 15], the pressure distribution computed on a spinnaker were compared with the pressure distributions measured on sails in the YRU wind tunnel and showed general similarities and some differences.
The main disadvantage of RANS is the lack of generality, i.e. the semi-empirical nature of the equations used to close the averaged Navies-Stokes (NS) equations. After time averaging the NS equations, a new unknown three-dimensional second-order symmetric tensor has to be solved: the Reynolds Stress Tensor. The turbulence model (TM) is the correlation structure between the mean flow and the Reynolds Stress. When RANS is used for modelling sail aerodynamics, the steady incompressible time-averaged NS equations are solved; the Reynolds Stress Tensor is modelled by means of the scalar turbulent viscosity, which can be expressed in several semi-empirical forms, leading to different TMs.
Since 2001 [16] it has been debates which TM performs better in terms of aerodynamic forces on sails: the results are generally controversial. As mentioned above, Hedges [10, 11] was the first investigator who performed a RANS analysis on downwind sails. She used a k-ε model, which was developed in her ME Thesis, for the analysis of a symmetrical spinnaker and mainsail. The sails were designed by North Sails New Zealand for the Whitbread 60' yacht *Winston*. Hedges compared the

computed aerodynamic coefficients with wind tunnel forces measured at 90° apparent wind angle (AWA), which is the supplementary angle between the wind and the boat directions. Several sail trims (different boom and pole angles) were tested to maximize thrust force. In the simulations the hull was not included. At AWA=90° the flow field was mainly attached and the TM could work adequately on the structured hexahedral grid.
Later Richter et al. [17] used a tetrahedral grid, with local refinement in the near wall region, but without any experimental comparison.
More recently, Lasher and Richards [13] did a deep investigation into International-America's-Cup-Class symmetrical spinnakers subjected to all 360° possible wind angles. The spinnakers were modelled in isolation without mainsail, rig and hull. The domain grid was made up of a number of tetrahedral cells of the order of 10^5. Three TMs were used: k-ε , k-ε realizable, and Reynolds Stress Model. The numerical results were then compared with wind tunnel tests. The authors reported the fragility of modelling the equilibrium atmospheric boundary layer, as the three TMs with the same inflow condition gave different velocity profiles at the model location. They calibrated the inflow turbulent kinetic energy inside an empty channel in order to obtain the same velocity profile at the model location for all the three TMs: inflow turbulent kinetic energy was decreased by 5% for the Reynolds Stress Model and by 20% for the k-ε realizable model, which was reported to be the most suitable one. One year later, Richards and Lasher [14] conducted some experiments with pressure measurements on the spinnaker and on the mainsail of an International America's Cup class 1:25 scale model. Measurements were performed for different sail trims at AWA=120°. The k-ε realizable model with a number of tetrahedral cells of the order of 10^5 was used for the CFD computations. A satisfactory agreement was found between numerical and experimental trends relatively to sail trims but both simulated pressures and forces suggested that the CFD reference dynamic pressure should be increased by 20%.
In the same year, Lasher and Sonnenmeier [18] modeled twelve symmetrical spinnakers using six TMs to compare results with wind tunnel data. Similarly to [13], the spinnakers were modelled in isolation while the mainsail, rig and hull were not considered. The grids were made up of a maximum of 330.000 tetrahedra. Without tuning the inflow turbulence parameters, they noticed that the force computations were almost insensitive to turbulent intensity and turbulent length scale, but for the k-ω family models a change in inflow turbulence intensity from 0.25% up to 2% significantly improved stability.
Significantly more detailed grids (up to 37 million tetrahedral elements) were used by Viola [12] for his study onto an America's Cup class yacht sailing downwind in light air, at AWA=45°, 105° and 120°, equipped with asymmetric spinnaker and mainsail. The hull, the mast and the boom were also considered in the simulation. The high grid resolution permitted squeezing the role of the TM and simulations without TM were performed. Lift and drag global coefficients exhibited a converging trend towards the experimental data with differences damped out at 3% for the highest grid resolution. Several TMs were also tested but no appreciable increase in accuracy was achieved and a general overestimation of forces was reported.
The present work deals with a further advance on what was achieved by Viola [12]. The role of the TM, when very high grid resolution is used, was investigated by means of numerical experiments. Simulations with grids spanning from 4 x 10^6 to 10^9 tetrahedral cells and with three numerical schemes with increased order of accuracy were performed without TM, while two TMs, k-ε realizable and k-ω SST, were tested with three grids spanning from 1.7 x 10^5 to 1.1 x 10^7 tetrahedral cells.

2. METHODS

2.1 GEOMETRIC MODEL

The geometry used by Viola [12] at AWA=45° was adopted in the present work. The flying shapes of the asymmetric spinnaker (on the left hand side in Figure 1) and of the mainsail (on the right hand side in Figure 1) were measured at the Politecnico di Milano Wind Tunnel with photogrammetric techniques.

Figure 1: Photograph of the America's Cup Class 1:12.5 scaled model during the wind-tunnel test.

The large test section (4 m height by 14 m wide) allowed a 1:12.5 model scale. The model was 2.7 m high, namely reference height *h* hereinafter. More details about the test section and the flow characteristics were published by Fossati et al. [19]. A twisted vane device, which can be observed upwind of the model in Figure 1, was used to twist the incoming flow and to model the change of the apparent wind velocity vector with the height. The onset flow at 0.8 m (10 m in full-scale) from the wind-tunnel floor is not deflected; while it is gradually deflected to the left below this height and to the right above this height. As a consequence, the angle of attack on the sails is decreased on the lowest sections and it is increased on the highest sections. Interested readers can find further details by Zasso et al. [20].

2.2 BOUNDARY CONDITIONS

The sails were modelled with zero thickness, while simplified models of the hull, mast and boom were drawn for the computations.
Inlet and outlet boundary conditions were imposed at 3.7 *h* windward and 7.4 *h* leeward with respect to the hull model, respectively.
The dynamic-pressure wind-tunnel vertical profile was measured above the force sensor in the empty test section. Conversely, it was not measured on a section to windward of the model when the physical model was present. Therefore, the dynamic-pressure vertical profile measured in the empty test section was integrated from the wind-tunnel floor up to the head of the mast and the computed value was adopted as inflow condition in the CFD analysis. Hence a uniform velocity profile in the direction of the longitudinal axis of the wind tunnel was used as inflow condition and, thus, the wind vertical profile was neglected. Moreover, the wind tunnel floor was modelled with a slip condition and thus the wind tunnel boundary layer was not modelled. This should be taken into account when numerical and experimental forces are compared but such an approach was necessary in order to investigate the effects of modelling the sail boundary layers and wakes with different grid resolutions. In fact, if a non-slip condition was used to model the wind-tunnel floor, and if a twisted and non uniform vertical velocity profile was used at the inlet, then different grid resolutions and numerical algorithms would have led to different onset conditions and thus to major differences in the aerodynamic sail forces.
When a TM was used, the inlet turbulence parameters k and ε or ω were correlated to a turbulence intensity of 2% and to a turbulent length scale of *h/14*.
A uniform zero reference pressure was imposed at the outlet boundary. The wind tunnel cross section - 5.2 *h* wide and 1.5 *h* high – was modelled using a sub-domain 4.4 *h* wide and 1.3 *h* high, modelling a lower wind-tunnel roof and a narrower test section, avoiding the need to model the wall velocity profile. Hence slip-conditions instead of non-slip-conditions were imposed at 2.2 *h* on both sides and at 0.3 *h* over the top of the model.

2.3 GRID GENERATION

Two sets of grids were performed. The grid generation process used to achieve the first set of grids is one of the innovative aspects of the present work. To reach a billion cell grid a very large amount of RAM is necessary (about 2 TB in our case), which is barely available in a single CPU and a reliable parallel grid generator was unknown to the present authors. For this reason a parallel building strategy was developed. The reconstructed sail shapes and a simplified model of the hull and rig were meshed with uniform triangular elements with the pre-processor *Gambit v2.4.6* (*Ansys Inc*.). Two grids were generated with triangle's edges of *h/190* and *h/380*, respectively. The other boundary surfaces were meshed with triangles of increasing size away from the meshed surfaces with a growth rate of 1.1 and with a maximum size of *h/5*. The two boundary grids obtained were imported into *Tgrid v5.0.6* (*Ansys Inc*.) and tetrahedral elements were generated from the surface grid. A 4-million-cell grid and a 16-million-cell grid were generated, respectively. The 16-million-cell grid required about 8 GB of RAM to be generated in a few seconds. To generate the larger grids a parallel process was necessary. To do this the 16-million-cell grid was imported into the solver *Fluent v6.3.35 beta* (*Ansys Inc.*) and partitioned into 512 parallel processes. Hence, each tetrahedron was subdivided into 8 tetrahedra using a hanging-node algorithm, obtaining a grid with 128 million cells already partitioned. By repeating this procedure a grid with 1.024 billion cells was obtained. At the end of this procedure four topologically similar grids were obtained, consisting of 4, 16, 128 and 1024 million tetrahedra and named '4M', '16M', '128M' and '1024M', respectively, in the following.
To the authors' knowledge this 1024M grid is the first computational grid on a complex fully three-dimensional geometry ever implemented with more than one billion cells.
The second set of grids was made with the two pre-processor *Gambit v2.4.6* and *Tgrid v5.0.6* (*Ansys Inc*.) without need of parallel refinement. A surface grid of triangles was made in *Gambit*, then 170,000 tetrahedra were extruded in *Tgrid* producing the base grid. A more refined grid was obtained by halving each edge of the tetrahedron, resulting in 8 new tetrahedra from each tetrahedron of the previous step. In this way, 3 grid sizes were generated with 1.7×10^5, 1.4×10^6, 1.1×10^7 cells, respectively, which are named '0.17M', '1.4M' and '11M' in the following. For the base grid, the edge of the triangle on the sail surface was *h/70*. A growth rate of 1.5 was used to stretch the nodes from the near wall region to the far field.

2.4 GRID RESOLUTION

The flow around the sails is mainly turbulent being the full-scale Reynolds number (*Re*) based on the yacht height of the order of 10^6. Wind tunnel experiments are usually performed at Reynolds numbers 10 times lower than full-scale Reynolds numbers because of the fragility of the model. The wind-tunnel tested $Re = 4 \times 10^5$ based on the height *h* was thus modelled numerically. Based on Kolmogorov dissipative scale, a number of cells of the order of $Re^{9/4} = 4 \times 10^{12}$ would allow the smallest turbulent scale to be computed. Versteeg and Malalasekera [21] noted that the grid cell requirement of $Re^{9/4}$ can be relaxed by two orders of magnitude. Therefore a 4×10^{10} cells should be able to compute all the necessary turbulent scales, from the largest which draw energy from the mean flow, to the smallest that are associated with viscous dissipation. In the present work up to 1×10^9 cells were used. Therefore, the highest resolution grid is only 40 times coarser than the grid needed to compute all the turbulent scales.

2.5 SOLVER SETTINGS

The incompressible Navier-Stokes equations with the above-mentioned boundary conditions were solved using *Fluent v6.3.35 beta (Ansys Inc.*), which is a finite volume solver. The implicit pressure-based steady formulation with the pressure-velocity-coupling scheme SIMPLE was used. Three discretization schemes were considered: first-order upwind for pressure and velocity ('p1v1' in the following), first-order upwind for pressure and second-order centered QUICK for velocity ('p1vq' in the following), second-order upwind for pressure and velocity ('p2v2' in the following). One of the aims of the present work was to investigate numerical schemes of higher order than the p1v1 scheme adopted in [12].
Under-relaxation coefficients were tuned to optimize converging time and to keep normalised residuals below 10^{-3}. The converging criterion was defined onto a signal analysis of the global lift and drag coefficients. The force coefficients were computed dividing the forces acting on the sails, hull and rigging, by the inflow dynamic pressure and the sail area. These were reported at each iteration and the computation was stopped after several oscillations around the mean values. For instance, Figure 2 shows lift and drag coefficients for each iteration divided by the average values computed on the regime iterations, in the case of the 1024M grid and p1vq scheme. After less than 10^4 iterations the coefficients reached a stable oscillating trend around the mean value. Figure 3 shows the oscillating coefficients subtracted the mean values and normalized with the standard deviation for the regime iterations without the initial transient. In this case, mean values were computed averaging over 23,000 - 10,000 = 13,000 iterations.
For each computation similar trends were plotted and the standard deviation was always below 1% with respect to the absolute value. The corresponding normalised residuals of the continuity equations and the three velocity components were all lower than 10^{-3}.
The simulations completed with the first set of grids were performed without TM. Conversely, the simulations completed with the second set of grid were performed both without TM and with the k-ε realizable and k-ω SST models (named 'rlz' and 'sst' in the following). In this latter case, wall functions are expressed as in the non-equilibrium formulation (Fluent User Manual, 2006).

2.6 HPC ENVIRONMENT

In order to reach the highly demanding computational costs related to the 1024M grid, the use of an HPC environment was needed. All the computations were performed on a Hewlett-Packard Linux cluster equipped with 208 dual-processor blade nodes with Intel Xeon 3.166 GHz quad-core CPUs, 16 GB/node. Total peak performance of the system approached 22 teraflops per second. At the time that the simulations were performed, the system was ranked number 135 on the top-500 list of supercomputers conducted by www.top500.org/list/2008/06/200. Due to the massive memory usage of the hanging-node algorithm, in accord with the hardware characteristics, only half of the available CPU's were used in each computational node. In particular all the computations were performed on 512 CPU's using 128 computational nodes. In the case of the 1024M grid a total of 2TB of RAM was occupied for about 170 hours of computation.

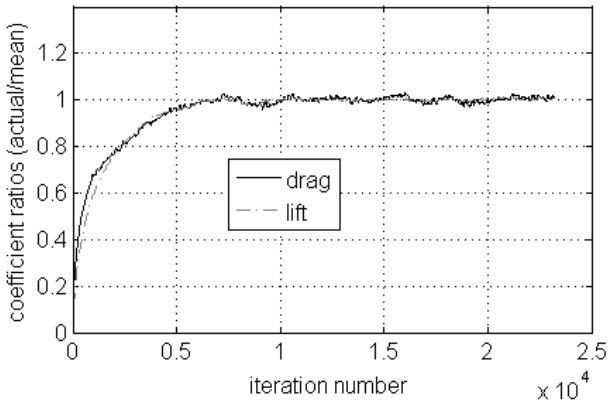

Figure2: Lift and drag coefficients divided by the mean values for all the computed iterations.

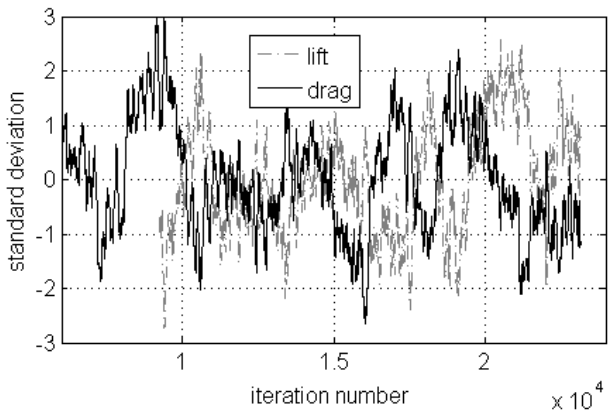

Figure 3: Lift and drag coefficients subtracted the mean values and normalized with the standard deviations for the regime iterations.

3. RESULTS WITHOUT TM

3.1 LIFT AND DRAG COEFFICIENTS

In this section, the results achieved without TM are presented. The results of twelve simulations performed with the first set of grids (4M, 16M, 128M, 1024M) and the three different algorithms (p1v1, p1vq, p2v2), are shown. The numerical/experimental ratios of the lift and drag coefficients are reported in Figure 4 and 5 respectively. The drag and lift coefficients computed with p1vq and p2v2 show asymptotic trends (even though only four grids are used to estimate the trends and thus more simulations should be performed to confirm the trends). Conversely, the fully first-order scheme shows a non-monotonic trend. The values of the lift and drag coefficients computed with p1v1, and the

decreasing trends when the grid accuracy increases up to 128M are in agreement with Viola [12].

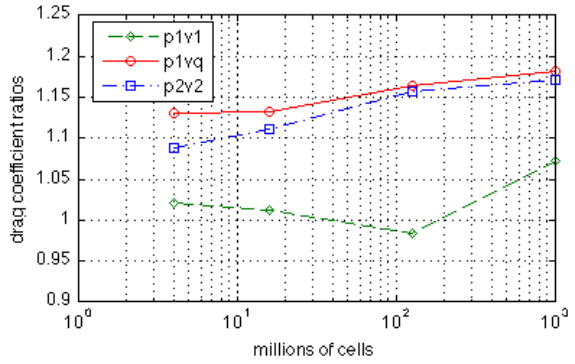

Figure 4: Drag coefficient ratio for the three algorithms versus the number of cells in logarithmic scale.

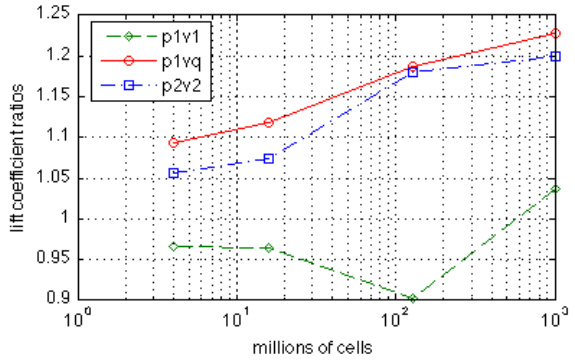

Figure 5: Lift coefficient ratio for the three algorithms versus the number of cells in logarithmic scale.

3.2 SEPARATED-FLOW REGIONS

The large amount of RAM needed to post-process pressure and velocity contours from the high grid resolution computations would have been untreatable. Hence the following analysis is focused on the 4 and 16 million cell grid computations. Figure 6 shows qualitative results for the cases 4M-p1v1, 4M-p1vq, 4M-p2v2, 16M-p1v1, 16M-p1vq, 16M-p2v2. The wind comes from the left hand side and the yacht is observed from the leeward side (suction side). Computed oil-flow lines (wall-bound streaklines) are visible on the leeward side of the asymmetric spinnaker, showing separated-flow regions.

In 4M-p1v1 (Figure 6a) separation occurs at the leeward side of the asymmetric spinnaker near the head (top corner) and the clew (aft-bottom corner). Increasing the computational accuracy, either in terms of grid resolution or in terms of algorithm resolution, the separated region enlarges near the head and decreases near the clew. Only the first order algorithm p1v1 does not follow this trend when the grid resolution increases. Hence, increasing the computational accuracy in terms of grid or algorithm resolution leads to a similar effect. Figure 4 and 5, show that increasing the computational accuracy, leads to larger force coefficients, with the exception of the p1v1 algorithm.

3.3 PRESSURE DISTRIBUTIONS

Local pressure analysis allows a better understanding of the grid and algorithm effects. Figure 7 gives results for test cases 4M-p1v1, 4M-p1vq, 4M-p2v2, 16M-p1v1, 16M-p1vq, 16M-p2v2 and shows the pressure coefficient (cp) along the normalized chord-wise coordinate for sections at z = 0.25 *h*, 0.5 *h,* 0.75 *h*, respectively, being z the vertical coordinate from the wind-tunnel floor.

On the leeward side, when the boundary layer is attached, cp decreases from the leading edge to about 1/3rd of the chord. Then it decreases until trailing edge separation occurs, and finally the pressure oscillates around a negative constant value up to the end of the chord. For instance, in Figure 7a on the lowest section (z = 0.25 *h*), trailing edge separation occurs at about 60% of the chord. Then cp oscillates around -1.1, presenting positive and negative peaks at about 65% and 75% of the chord respectively.

Focusing on the leeward side of the sail, increasing the computational accuracy leads to enhanced suction at the lower section (z = 0.25 *h*), and to a more oscillating cp trend at the higher section (z = 0.75 *h*), as due to a separated boundary layer. This explains why force coefficients increase when the numerical accuracy increases. In fact, increasing the numerical accuracy leads to lower cp's on the lowest section (due to a smaller separated region), while no significant differences are observed on the highest sections. Therefore, increasing the numerical accuracy leads to higher force coefficients because of the enhanced suction on the lowest section. This also explains why the coefficients computed with p1v1 decrease when the grid accuracy increases from 4M to 16M (Figure 4 and 5). In fact, as showed in Figure 6, only in the simulations performed with p1v1, the separated region near the clew does not decrease when the grid accuracy increases.

Wind-tunnel pressure measurements [24] show that the time-averaged cp is constant along the chord in the separated region. The steady simulations were unable to compute a constant time-averaged cp along the chord in the separated region and, conversely, showed oscillations along the chord.

Focusing on the highest of the three sections (z = 0.75 *h*), Figure 7 shows that for every grid and algorithm, the flow is separated and cp shows oscillations along the chord. Figure 8 shows contours of cp in the horizontal plane z = 0.75 *h* for test cases 4M-p1v1, 4M-p1vq, 4M-p2v2, 16M-p1v1, 16M-p1vq, 16M-p2v2. The wind comes from the left and the spinnaker and the mainsail sections can be observed. Increasing the computational accuracy, either in terms of grid or algorithm resolution, allows for solving finer convective nucleus and hence leads to a more oscillating boundary layer.

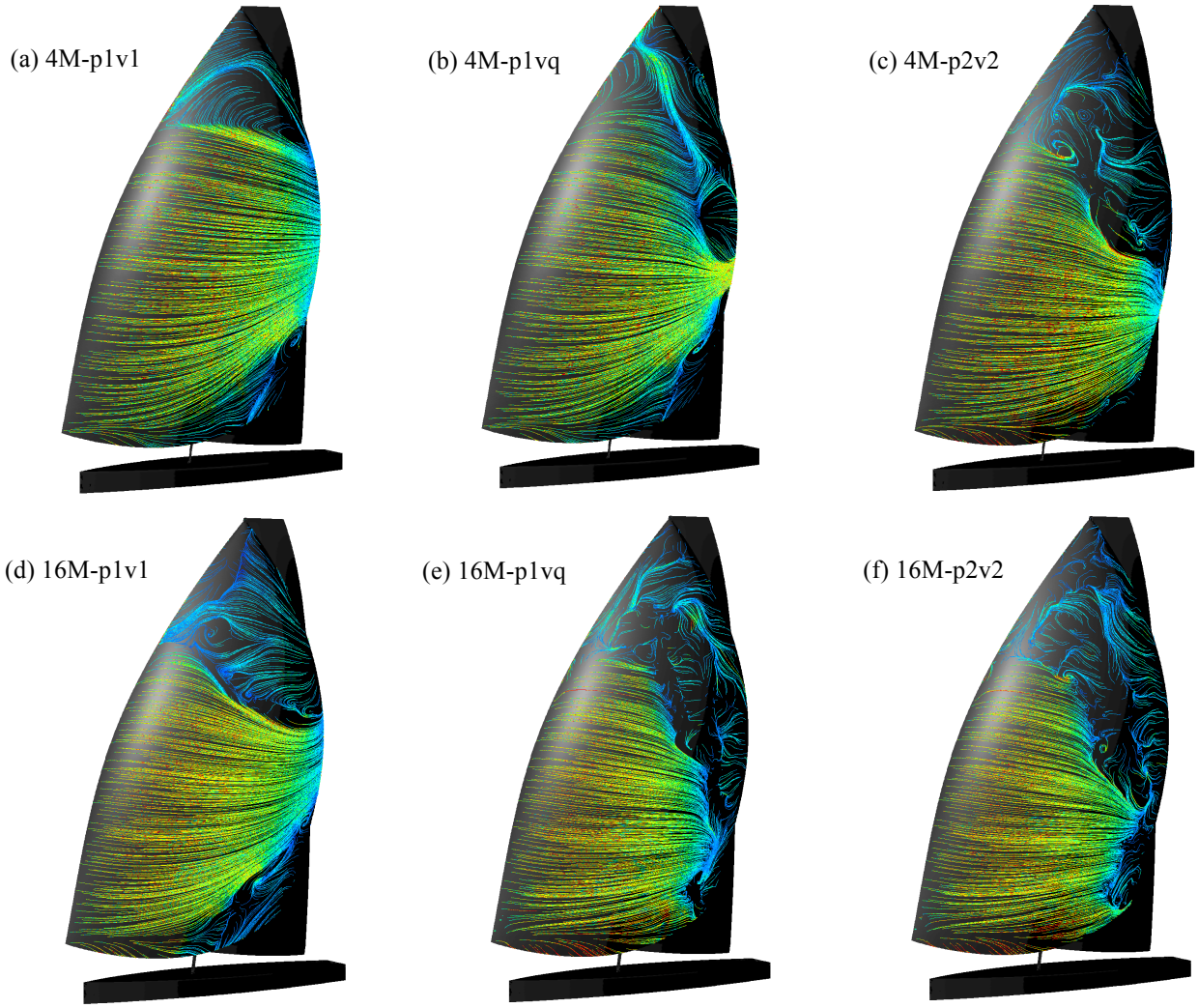

Figure 6: Computed oil-flow lines on the leeward side of the spinnaker for three algorithms and two grid sizes.

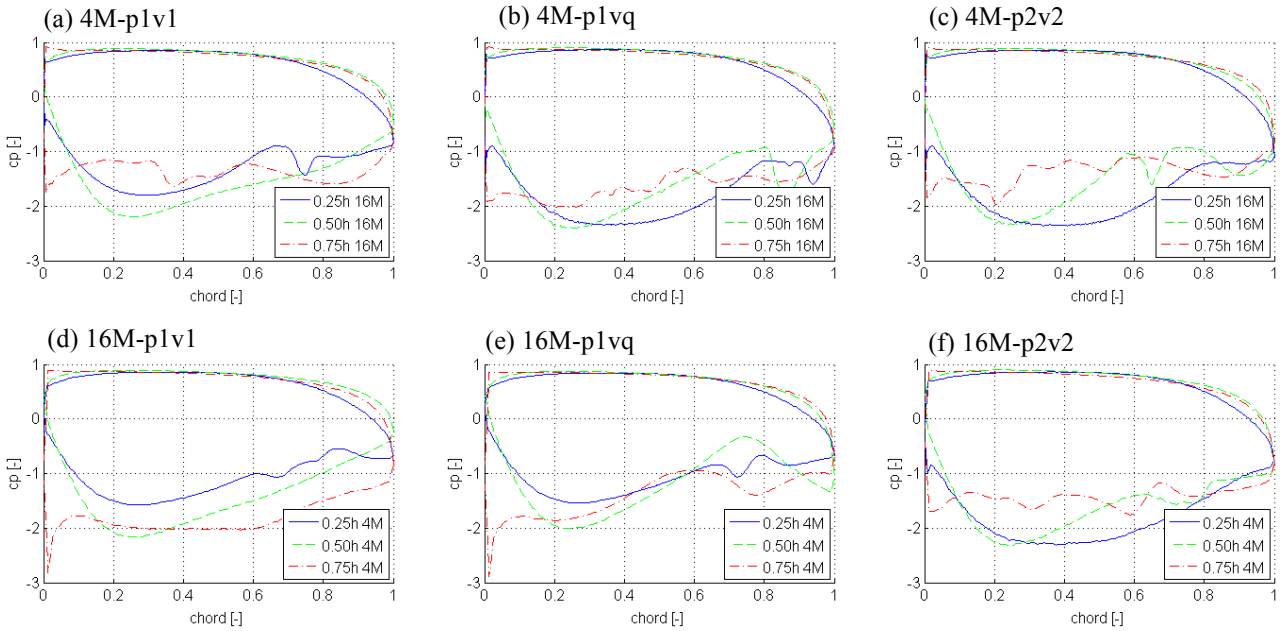

Figure 7: Pressure coefficient cp along the non-dimensional chord-wise coordinate of the spinnaker at three horizontal heights (0.25 *h*, 0.5 *h*, 0.75 *h*), for three algorithms and two grid sizes.

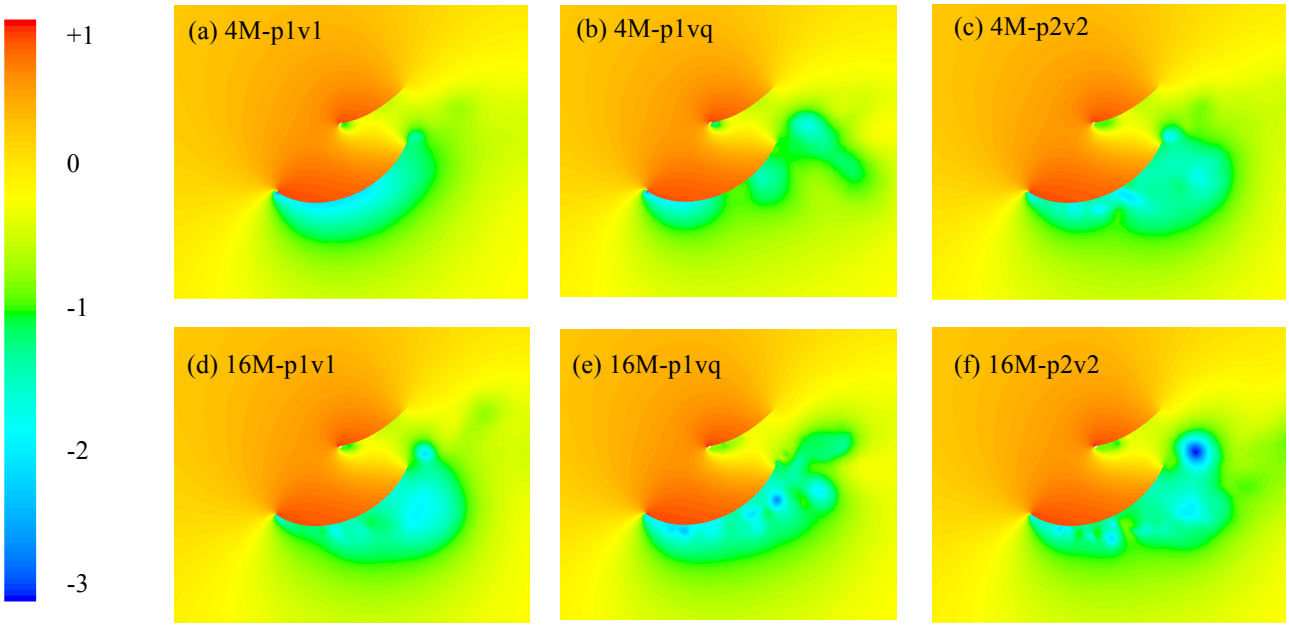

Figure 8: Pressure coefficient contour on a horizontal plane at 0.75 *h*, for three algorithms and two grid sizes.

4 COMPARISON WITH TM

In this section the results achieved with and without TM with the coearser set of grids (0.17M, 1.4M and 1.1M) are presented. Simulations without TM (named 'noTM' in the following figures) were performed both with p1v1 and p1vq, while simulations with the rlz and sst models were performed with p1vq.

Figures 9 and 10 shows the numerical/experimental lift and drag coefficient ratios across the 3 grids. Results for the simulations without TM are in good agreement with the results achieved on the higher-resolution set of grids (Fig. 4-5), and results for the simulations without TM with p1v1 scheme are in good agreements with [12]. The sst model over-estimated significantly the drag coefficient and the curve in Figure 10 was decreased by 0.2 to avoid stretching the scale. The sst model was presented by Menter [23] in order to be integrated to the wall and thus it shows worse performance than the rlz model when used with wall fuctions. The larger drag over-estimation by the sst model than the rlz model was also reported by [12].

Without TM, coefficients show opposite trends when computed with different schemes, and their values vary significantly when the grid resolution is increased. Conversely, the force coefficients computed with the TM show almost linear decreasing trends.

Increasing the grid resolution, the simulations performed without TM compute finer convective nuclei leading to pressure oscillations in the separated regions. For instance, Figure 11 shows the pressure contours at z = 0.75 *h* computed on the 3 grids without TM and with the rlz model. The simulations performed with the rlz model do not present significant differences when the grid resolution is increased. Similar results are achieved with the sst model and thus are not presented.

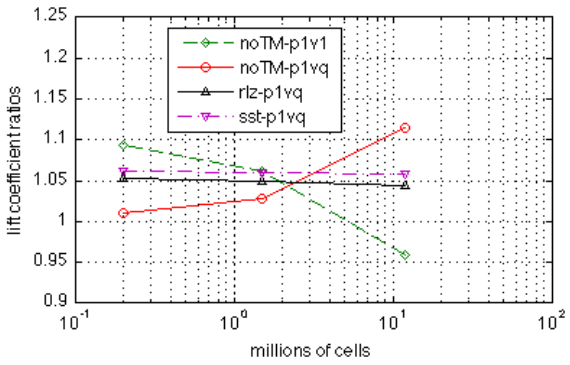

Figure 9: Lift coefficient ratio for the three turbulence treatments and two algorithms versus the number of cells in logarithmic scale.

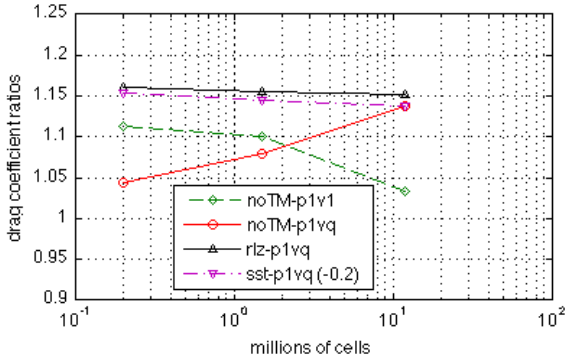

Figure 10: Drag coefficient ratio for the three turbulence treatments and two algorithms versus the number of cells in logarithmic scale.

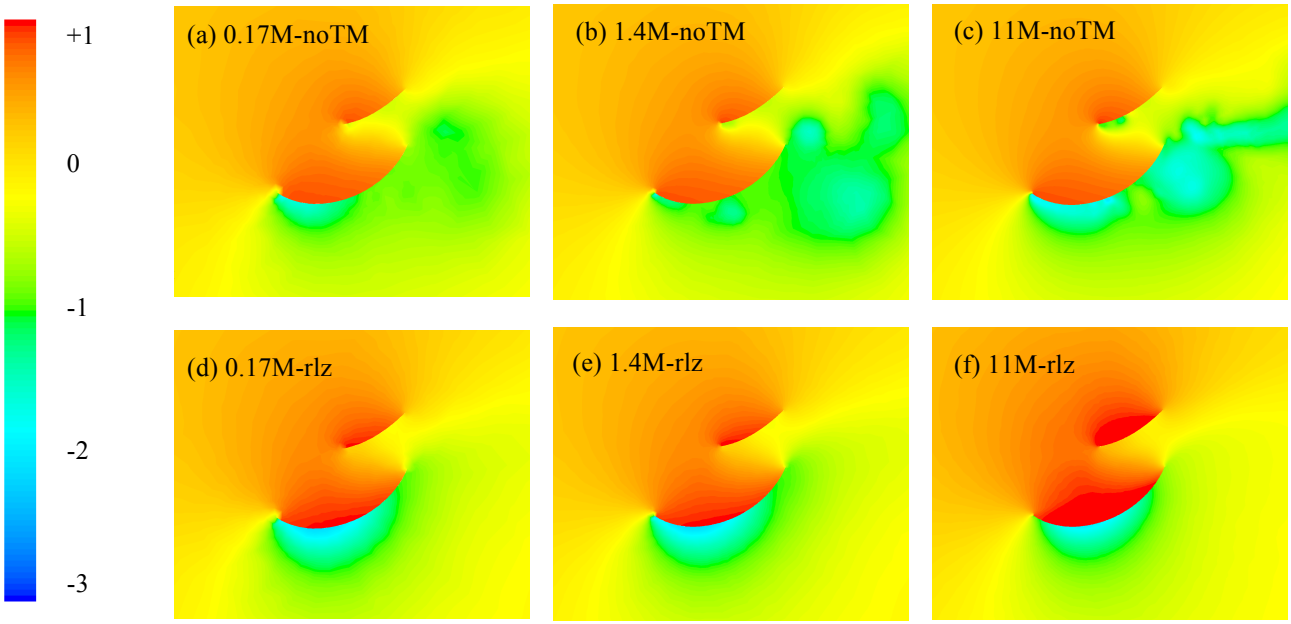

Figure 11: Pressure coefficient contour on a horizontal plane at 0.75 *h*, for three grid sizes without TM and with the rlz model. Wind comes from the left, the spinnaker and mainsail sections can be observed.

5 DISCUSSION

5.1 RESULTS WITHOUT TM

Viola [12] observed that when grids with a number of cells of the order of 10^7 were used - squeezing the role of the TM - simulations without TM led to a good agreement between the numerical and experimental force coefficients, and using a TM did not lead to more accurate results. A first order accuracy numerical scheme was used to achieve more stable solutions.

These results motivated the present work, where more refined grids and higher order algorithms are investigated without TM. The computed values of lift and drag coefficients and their trends with the grid resolution are in agreement with what observed by Viola. However, the present investigation shows that increasing the numerical accuracy further or increasing the order of the algorithm leads to the opposite trend. Figures 4 and 5 show that, increasing the grid accuracy and using the p1v1 algorithm, force coefficients decrease with low-resolution grids, but then they increase when the one-billion-cell grid is used. If higher order algorithms are used, force coefficients increase monotonically.

Figures 6-8 show that the force coefficient over-estimation is not correlated with a uniform increase of a global index, such as the dynamic pressure or the angle of attack. Indeed, it is correlated with latter trailing edge separation and thus with enhanced suction on the lowest sections of the spinnaker. Therefore a different geometry could lead to the opposite trend.

The asymptotic trends of the force coefficients when the grid resolution increases (Fig. 4-5), show the diminishing effect of the second order numerical diffusion due to the grid. In fact, the fully second-order algorithm p2v2 shows the strongest asymptotic attitude. Conversely, the fully first-order algorithm p1v1 is more affected by numerical diffusion and presents less consistent trends but, with high grid resolution, shows a converging trend towards results from the higher order algorithms.

With very high grid resolution and thus low numerical diffusion, force coefficients are over-estimated by about 20% (Fig. 4-5). This can be due to the following reasons or to the combination of them.

Force coefficient overestimation can be due to the different inlet condition between the experimental setup and the numerical model. In fact, the experimental non-uniform vertical profiles of the dynamic pressure and wind direction were not modelled, and so was the wind tunnel boundary layer. As explained in Section 2.2, this approach can lead to larger differences between numerical and experimental results but allows a better understanding of the force coefficient trends.

Non-solving the time-dependent term of the momentum equation, which represents energy exchange between the local and the advective accelerations, leads to an additional constraint, which partially inhibit the energy flow and might accentuate the force coefficient overestimation. Figure 8 shows that in the separated regions, the higher the numerical accuracy the more convective nuclei are modelled. In these regions the flow is unsteady and the simulations, which do not solve the time-dependent term, are unable to model the unsteady pressure and velocity fields. At every iteration, the solution is neither an averaged solution nor an instantaneous solution, but it is an approximate solution.

As a final observation, the one-billion-cell grid allows account to be taken of turbulent scales with a wavelength of the order of the resolution grid size. In the model region, the grid size is of the order of $h/10^4$ and the wind

speed is about 1 *h* per second, consequently the highest resolution grid takes into account fluctuations of the order of 10^4 Hz, which is two orders of magnitude higher than the sampling frequency in the wind tunnel force measurements. Consequently averaged forces might be affected by the highest frequency fluctuations that are filtered in the experimental measurements.

5.1 RESULTS WITH TM

The high Reynolds number leads to a lack of grid points which would be necessary to compute the smallest turbulent dissipative eddy. In fact, as said in Section 2.6, even the one-billion-cell grid is about 40 times too coarse to model all the turbulent scales. Therefore the grid operates like a cut-off filter that chops out the lower scales. Consequently, an energy barrier in the spectral space can produce an excess of energy close to the grid scale. In particular, in the region far from the model, e.g. in the upwind region, the relatively poorer grid size cannot adequately transport and dissipate turbulent quantities. When a TM is used and turbulent flow is modelled at the inlet, the turbulence entering into the domain introduces additional energy into the computational domain, which might not be adequately dissipated because of the lack of spatial resolution. This might lead to over-estimation of the dynamic pressure and thus of the aerodynamic forces. This can explain why, both in the present work (Fig. 9-10) and in other author's works [13, 14], force coefficients are over-estimated when a TM is used with a number of cells of the order of 10^6 and with a low-order numerical scheme.
When the grid resolution is increased, the energy flow through more turbulent scales and it is better dissipated, leading to a lower force over-estimation. Therefore, increasing the grid resolution leads to decreasing trends of the force coefficients (Fig. 9-10).
The present results show that grid resolution required to achieve a grid-independent solution in downwind sail aerodynamics is very high. The second set of grids doesn't show a grid independent solution and grid resolution or accuracy of the numerical scheme should be further increased.
TM allows time-averaged solutions to be computed. For instance, a constant pressure along the sail chord downstream of trailing edge separation is computed (Fig. 11), in agreement with experimental observations [22].

6 CONCLUSIONS

In the present work the aerodynamics of an America's Cup Class yacht, sailing with asymmetric spinnaker and mainsail at 45° apparent wind angle, was investigated with a CFD code. The trim condition previously tested in the wind tunnel was considered here.
The present work deals with a further advance on what was achieved by Viola [12], who observed that using high resolution grids with up to 3.7 x 10^7 cells and not modelling the Reynolds Stress Tensonr led to good agreement with the experimental data, and solving two additional turbulence model equations did not increased the simulation accuracy. The aim of the present paper is evaluating the role of the turbulence model when high grid resolution is used and its role is squeezed. The performance of steady simulations completed with and without turbulence model are investigated across a wide range of grid resolutions and three numerical schemes with increasing accuracy.
Two sets of grids were performed. Each set presented topological similar grids achieved halving the node distance at every refinement. The first set of grids span from 4 x 10^6 to 10^9 cells, while the second set span from 1.7 x 10^5 to 1.1 x 10^7. Both first and second order accuracy upwind schemes, and second order accuracy QUICK scheme were tested. Simulations with two different turbulence models, k-ε realizable and k-ω SST, and without turbulence model were performed.
The experimental lift and drag force coefficients were compared with the values computed with the different grids, the three algorithms, and the different turbulence treatments.
Simulations performed without turbulence model with the first set of grids showed the following results:

- Increasing the numerical accuracy, either increasing the grid resolution or increasing the algorithm order, leads to numerical diffusion decrease and to asymptotic trends across the grids and the numerical schemes of the global aerodynamic force coefficients.

- With high numerical accuracy, force coefficients are over-estimated by about 20%, which can be due to the neglected vertical inflow velocity profile and wind-tunnel boundary layer, and to the neglected unsteady terms which doesn't allow a time-averaged solution to be computed.

- The force over-estimation is not correlated with an overall increase of a global index (e.g. the dynamic pressure), while it is correlated with the enhanced suction on the lowest section of the spinnaker and thus it the specific of the modelled geometry.

The comparison between the simulations performed with and without turbulence model on the second set of grids showed the following results:

- Force coefficients were over-estimated with turbulence model, which can be due to the neglected vertical inflow velocity profile and wind-tunnel boundary layer, and to the insufficient grid resolution and low accuracy of the numerical scheme leading to an excess of energy and to a non adequate dissipation of the additional turbulent quantities introduced at the inlet.

- Simulations performed with a turbulence model showed consistent decreasing trends of the force coefficients when the grid resolution was increased but a grid independent solution was not achieved, showing the need of further grid refinement or higher order numerical scheme.

While force coefficients are expected to decrease asymptotically to the experimental values if the numerical accuracy is increased using a turbulence model, when both the time-dependent terms and the Reynolds stress tensor are neglected, increasing the numerical accuracy leads to non-consistent trends, which depends on the specific modelled geometry.
The wide range of tested grids shows that grid independent solutions with low-accuracy-order numerical schemes can be found only when very high grid resolution is used. However, using the turbulence model and halving the node distance led to very small force coefficient differences, suggesting that particular caution should be used when a grid-independent solution is estimated.
As a closing remark, considering the role of numerical 'experiments' into sailing yacht design and their interplay with traditional environments, the considerable computational and modelling efforts provided within the present work are a proof of concept of both the enormous perspectives of viscous computational fluid dynamics and of the relevant technological limiting factors nowadays present in this field of application.

7 ACKNOWLEDGMENTS

The authors want to thank all the people that have been involved in the great challenge to perform and solve the first one-billion-grid on a fully 3D complex geometry (other authors have previously reached this challenge but by joining several smaller grids together or by dealing with simply cubic geometries): Claudio Arlandini, Marco Pirola, Paolo Ramieri, Paride Dagna, Silvia Bozzi. Giuseppe Passoni is gratefully acknowledged for his support and expert suggestions.

8 REFERENCES

1. GRAF K., BOHEM C., RANZSCH H., 'CFD- and VPP-Challenges in the Design of the New AC90 America's Cup Yacht', in the proceedings of the 19th Chesapeake Sailing Yacht Symposium, pp. 1-17, Annapolis, USA, March 20th-21st, 2009.

2. BRAUN J.B., 'High Fidelity CFD Simulations in Racing Yacht Aerodynamic Analysis', in the proceedings of the 3rd High Performance Yacht Design Conference, pp. 168-175, Auckland, New Zealand, December 2nd-4th, 2008.

3. HUTCHINS N., 'The Use of Ansys CFX in America's Cup Yacht Design', in the proceedings of the 3rd High Performance Yacht Design Conference, pp. 185-192, Auckland, New Zealand, December 2nd-4th, 2008.

4. MILGRAM J.H., 'The Aerodynamics of Sails', In the proceedings of the 7th Symposium of Naval Hydrodynamic, pp. 1397-1434, 1968.

5. MILGRAM J.H., 'The Analytical Design of Yacht Sails', in SNAME annual meeting, vol. 13, pp. 118-160, 1968.

6. GENTRY A.E., 'The Application of Computational Fluid Dynamics to Sails', in proceedings of the Symposium on Hydrodynamic Performance Enhancement for Marine Applications, Newport, Rhode Island, USA, 1988.

7. FALLOW J.B., 'America's Cup Sail Design', Journal of Wind Engineering and Industrial Aerodynamics, 63, 183-192, 1996.

8. CLAUGHTON A.R., CAMPBELL I.M.C., 'Wind Tunnel Testing of Sailing Rigs', in the proceedings of the International HISWA Symposium on Yacht Design and Yacht Construction, pp. 89-106, Amsterdam, November 14th-15th, 1994.

9. QUERARD A.B.G., WILSON P.A., 'Aerodynamic of Modern Square Head Sails: a Comparative Study Between Wind-Tunnel Experiments and RANS Simulations', in the proceedings of In the Modern Yacht, Southampton, UK, 2007.

10. HEDGES K.L., 'Computer Modelling of Downwind Sails', ME Thesis, University of Auckland, New Zealand, 1993.

HEDGES K.L., RICHARDS P.J., MALLISON G.D., 'Computer Modeling of Downwind Sails', Journal of Wind Engineering and Industrial Aerodynamics, 63, 95-110. 1996.

12. VIOLA I.M., 'Downwind Sail Aerodynamics: a CFD Investigation with High Grid Resolution', Ocean Engineering, vol. 36, issues 12-13, pp. 974-984, 2009.

13. LASHER W.C., RICHARDS P.J., 'Validation of RANS Simulations for International America's Cup Class Spinnaker Force Coefficients in an Atmospheric Boundary Layer', Journal of Ship Research, 51 (1), 22–38, 2007.

14. RICHARDS P.J., LASHER W.C., 'Wind Tunnel and CFD Modelling of Pressures on Downwind Sails', in the proceedings of VI International Colloquium on Bluff Bodies Aerodynamics & Applications, Milan, Italy, July 20th-24th, 2008.

15. VIOLA I.M., FLAY R.G.J., 'Pressure Distribution on Sails Investigated Using Three Methods: On-Water

Measurements, Wind-Tunnel Measurements, and Computational Fluid Dynamics', in the proceedings of the 20th Chesapeake Sailing Yacht Symposium, Annapolis, MD, USA, March 18th-19th, 2011.

16. COLLIE S.J., GERRITSEN M., JACKSON P., 'A Review of Turbulence Modelling for Use in Sail Flow Analysis. School of Engineering', report no. 603, Auckland, New Zealand, 2001.

17. RICHTER H.J., HORRIGAN K.C., BRAUN J.B., 'Computational Fluid Dynamics for Downwind Sails', in the proceedings of the 16th Chesapeake Sailing Yacht Symposium, Annapolis, USA, 2003.

18. LASHER W., SONNENMEIER J., 'An Analysis of Practical RANS Simulations for Spinnaker aerodynamics', Journal of Wind Engineering and Industrial Aerodynamics, 96, 143–165, 2008.

19. FOSSATI F., MUGGISCA S., VIOLA I.M., ZASSO A., 'Wind Tunnel Techniques for Investigation and Optimization of Sailing Yachts Aerodynamics', in the proceedings of the 2nd High Performance Yacht Design Conference, Auckland, New Zealand, pp. 105-113, February 14th-16th, 2006.

20. ZASSO A., FOSSATI F., VIOLA I.M., 'Twisted Flow Wind Tunnel Design for Testing Yacht Sails', in the proceedings of EACWE4 European and African Conference on Wind Engineering, Prague, Czech Republic, July 11th-15th, 2005.

21. VERSTEEG H. K., MALALASEKERA W., 'An Introduction to Computational Fluid Dynamics - The Finite Volume Method', 2nd edition, Pearson Education, 2007.

22. VIOLA I.M., FLAY R.G.J., 'Pressure Distribution on Modern Asymmetric Spinnakers', International Journal of Small Craft Technology, Trans. RINA, vol. 152, part B1, pp. 41-50, 2010.

23. MENTER F.R., 'Two-Equation Eddy-Viscosity Turbulence Models for Engineering Applications', AIAA Journal, vol. 32 (8), pp. 1598-1605, 1994.

9. AUTHORS BIOGRAPHY

Ignazio Maria Viola holds the current position of Lecturer in Naval Architecture at the School of Marine Science and Technology of the Newcastle University in UK. Ignazio's specialist skills and experience are in numerical and experimental fluid dynamics. His main research focus is high-performance sailing yachts and, in particular, sail aerodynamics and hull hydrodynamics. He is member of the Yacht Research Unit at the University of Auckland where he performed a Post Doctoral Fellow collaborating with the America's Cup Team Emirates Team New Zealand. He was awarded a PhD at the Politecnico di Milano Wind Tunnel, (funded by the Luna Rossa Challenge for the 32nd America's Cup) for a thesis on the numerical and the experimental analysis of America's Cup sail plans. His research portfolio also includes the aerodynamics of trains, cars, long- span bridges and tall buildings. Since graduating as a Naval Engineer from the Università degli Studi di Genova in 2001, he has performed several engineering consultancies for various marine industries.

Raffaele Ponzini holds the current position of CFD expert at CILEA computer centre. His working domain includes also teaching C, C++, Python and object oriented programming technique. In 2007 he finished his PhD program (cum Laude) in Bioengineering at the Politecnico di Milano. His research interests include multiscale models in hemodynamics, and scientific visualization. He's author of 15 peer reviewed international papers in the field of biomechanics and computational fluid dynamics.